Journal of Molecular Liquids 384 (2023) 122283

Contents lists available at ScienceDirect

Journal of Molecular Liquids

journal homepage: www.elsevier.com/locate/molliq

Effective adsorptive removal of tetracycline from aqueous solution by Zn-BTC@SBC derived from sludge:Experimental study and density functional theory (DFT) calculations

Zhikang Deng [a,1], Jinyao Zhu [a,1], Ping Li [b,*], Zhenjie Du [b], Xuebin Qi [b], Xi Chen [a], Rui Mu [a], Chenyu Zeng [a], Yongfei Ma [a,*], Zulin Zhang [a,c,*]

[a] Hubei Key Laboratory of Mineral Resources Processing and Environment, School of Resources and Environmental Engineering, State Key Laboratory of Silicate Materials for Architectures, Wuhan University of Technology, Wuhan 430070, China
[b] China-UK Water and Soil Resources Sustainable Utilization Joint Research Centre, Farmland Irrigation Research Institute, Chinese Academy of Agricultural Sciences, Xinxiang 453002, China
[c] The James Hutton Institute, Craigiebuckler, Aberdeen AB15 8QH, UK

ARTICLE INFO

Keywords:
Zn-BTC@SBC
Tetracycline
Adsorption
Regeneration

ABSTRACT

Overuse of tetracycline (TC) has caused serious damage to aquatic environment. Developing sustainable and efficient removal technologies for TC is of great significance to eliminate its ecological risks. In this study, a novel zinc metal organic framework porous biochar composite (Zn-BTC@SBC) derived from sludge was the first time synthesized and employed for adsorptive removal of TC from water.

The adsorption process of TC followed the Elovich and Temkin model and the maximum capacity of Zn-BTC@SBC to adsorb TC was 125.9 mg/g. Characterization analysis demonstrated that the greater adsorption capacity of Zn-BTC@SBC was ascribed to its larger surface area, pore volume and abundant oxygen-containing functional groups. The fitting results showed that both chemisorption and physical adsorption predominated the adsorption process of TC on Zn-BTC@SBC. Further material characterization (FTIR and XPS) and density functional theory (DFT) calculations at the molecular level suggested that the good adsorption performance of Zn-BTC@SBC on TC might be due to chemisorption dominated by oxygen-containing functional groups, which included π-π conjugation, H-bonding and electrostatic interaction. And it was a spontaneous, endothermic and randomness increasing reaction. Both ion species/strength and solution pH significantly affected the adsorption capacity of Zn-BTC@SBC for TC. The natural water samples with complex composition (lake and river water) still showed 71.27–76.37 % of TC adsorbed. The used Zn-BTC@SBC was capable of maintaining its stable adsorption capacity by NaOH regeneration. This study demonstrated that Zn-BTC@SBC was a promising practicability in removal of TC and workable approach for sustainable utilization of sludge.

1. Introduction

Nowadays, the overuse of antibiotics has aroused the broad attention in China because it shares over 50 % of total antibiotics consumption in the world each year [1]. Among them, tetracycline (TC) has been widely used in the prevention and treatment of various diseases in humans and animals caused by bacterial infections due to its board-spectrum [2,3]. After use, about 80 % of the unmetabolized TC would be released into aquatic environment via human excretion [4]. The unsatisfactory removal efficiency of TC by the conventional wastewater treatment technologies resulted in frequent and wide detection in wastewater and natural waters (e.g., surface and underground water) [1,5,6]. TC residues would increase the bacterial resistance, resulting in incurable infections [7,8]. Hence, it was urgent to develop the efficient technology for TC elimination.

Different methods including catalytic oxidation [9,10], membrane separation technology [11], biodegradation [12] and adsorption [13,14] have been studied to eliminate TC in aquatic environment. Adsorption method has attracted extensive attention because of its low cost, simple operation and no toxic by-products [15]. Particularly,

* Corresponding authors.
E-mail addresses: firilp@163.com (P. Li), yongfei.ma@whut.edu.cn (Y. Ma), Zulin.Zhang@hutton.ac.uk (Z. Zhang).
[1] These authors contributed equally to this work.

https://doi.org/10.1016/j.molliq.2023.122283
Received 11 March 2023; Received in revised form 28 May 2023; Accepted 5 June 2023
Available online 10 June 2023

developing the efficient adsorbent was critical to facilitate the practical application of adsorption technology. Sludge was an unavoidable solid waste from wastewater treatment plants, and the annual production of sludge has been more than 6.0×10^7t in China in 2019 [16]. With high organic matter content, sludge was a promising feedstock for the production of porous biochar [17]. Using sludge as the raw material to produce carbon-based adsorbent could not only reduce its pollution (e.g., air and groundwater pollution) caused by the current main disposal approaches of incineration and landfill, but also realize its resource utilization [18–20]. While the large scale application of sludge biochar (SBC) was still limited by poor adsorption performance [21,22]. Herein, various methods (e.g., acid, alkali, metal salts and *N*-doping) had been used to enhance the physicochemical characteristics (e.g., porous structure, oxygen-containing functional groups and graphite degree) of SBC for its adsorption capacity enhancement [23–25].

Recently, metal–organic frameworks (MOFs) have attracted special concern as an adsorbent material because they are a class of crystalline microporous materials rich in well-defined channels, large specific surface areas, organic ligands and metals [26]. Among them, the organic ligand 1,3,5-benzenetricarboxylate (BTC) was considered as one of universal versatile ligands for MOFs construction due to its abundant binding sites with a coordination mode in all three directions [27]. The metals of Cu and Zn were proved to be optimal choices for constructing MOFs, and the most popular example was a MOFs of $[Cu_3(BTC)_2(H_2O)_3]_n$ (HKUST-1) which was constructed by the $(BTC)^{3-}$ unit [27]. Numerous MOFs have been synthesized to replace the Cu with other transition-metal ions, especially with Zn [28]. Zinc metal as MOFs were with relatively thermodynamic stability, strong coordination bonds, and entropy factor. In addition, the presence of Zn was more effective than that of Cu in increasing the specific surface area of the adsorbent due to the partial evaporation of Zn during the high-temperature hydrothermal process [23,29–31]. While the microporous structures was the main porous structure of the MOFs constructed by the $(BTC)^{3-}$ and Zn (e.g., Zn-BTC), which led to debilitate adsorption affinity, especially in high concentrations of organic pollutants removal [26]. To deal with this, the composite constructed with Zn-BTC and SBC (Zn-BTC@SBC) had potential to develop a microporous-mesoporous composite material and the composite would performed the superiority of both Zn-BTC and SBC [32]. Herein, inspired by these possibilities, the microporous-mesoporous porous structure was synthesized by Zn-BTC and SBC to provide a new-generation and environment friendly antibiotics adsorbent.

Notably, the biochar composites synthesized with MOFs were mainly used for adsorption of volatile organic compounds (VOCs) [26,27,33,34], which were rarely employed to adsorb organic pollutants from water, especially for emerging pollutants (e.g.,TC). On the other hand, previous works focused only on the "adsorption effect" (concentration change) without further studies, such as the analysis of the adsorption mechanism only by characterization qualitatively (physical adsorption or chemical adsorption). Few studies have evaluated the quantum chemical parameters of TC and adsorbents based on the Density Functional Theory (DFT) calculations to understand its reactivity at the molecular level. Therefore, the purpose of this work was to (1) synthesize Zn-BTC@SBC by one-pot hydrothermal method and investigate its adsorption capacity for TC; (2) identify the main adsorption mechanisms of Zn-BTC@SBC for TC by characterization and models fittings (kinetics, isotherms and thermodynamics; (3) study the critical environmental factors affecting the adsorption process of TC onto Zn-BTC@SBC; (4) evaluate the sustainable adsorption performance of the used Zn-BTC@SBC by NaOH regeneration; (5) verify the adsorption performance of Zn-BTC@SBC for TC in environmental waters; (6) investigate of TC adsorption mechanism on Zn-BTC@SBC by characterization and DFT calculations.

2. Materials and methods

2.1. Chemicals

TC ($C_{22}H_{24}N_2O_8$, CAS Number: 60–54-8, purity > 98 %) and all the other chemicals (e.g., NaOH, NaCl, $CaCl_2$) used in this study were of analytical grade or higher. All the above listed reagents were purchased from Aladdin Chemical Co. (Shanghai, China).

2.2. Synthesis of SBC and Zn-BTC@SBC

Sludge biochar (SBC) was prepared using the method previously reported [35]. Zn-BTC@SBC was prepared by one-pot hydrothermal method. In detail, 1.60 g SBC, 0.80 g $ZnCl_2$ and 0.80 g H_3BTC were injected into a Teflon reactor containing ethanol ($V_{ethanol} = 25$ mL) and dimethylformamide (DMF) ($V_{DMF} = 50$ mL), then it was sonicated for 30 min to develop a homogeneous mixture. Immediately after, the solution was transported into an oven for hydrothermal process for 1440 min at the specific temperature of 383 K. After that, this sample was cooled to the room temperature and cleaned by washing with ethanol and ultrapure water, which was dried at 333 K, milled and sieved (0.15 mm), and it was labelled as Zn-BTC@SBC.

2.3. Batch experiments

The kinetics, isotherms, thermodynamics, effects of pH, ionic species/strength and humic acid concentration were conducted to investigate the adsorption behaviors of TC onto Zn-BTC@SBC. The equations and parameters of kinetics (pseudo-first-order (PFO), pseudo-second-order [36] and Elovich), isotherms (Langmuir, Freundlich, Temkin and Dubinin–Radushkevich (D-R)) were summarized in Text S1. The pH, ionic species/strength, humic acid concentration, and regeneration with detailed reaction conditions were listed below. The experiments were conducted varying the following parameters: TC initial concentration (20 mg/L), adsorbent dose (0.04 g), solution pH (3–11), temperature (298 K), contact time (0–1440 min), cation species present (Na^+ and Ca^{2+}, the concentration was 1–100 mM), and HA concentration (1–10 mg/L). The total volume of the above experiment is 0.1 L using erlenmeyer flask. As for regeneration, Zn-BTC@SBC with attached TC were treated with ultrapure water, ethanol, and 0.1 mol/L NaOH. This process was repeated 3–10 times and the Zn-BTC@SBC were then reused. TC initial concentration, contact time, and temperature are consistent with the above experimental conditions, the adsorbent dose was adjusted to 0.2 g, and the total volume was 0.5 L. Furthermore, the characterization of adsorbents were given in Text S2.

2.4. DFT calculation

Duo to TC and biochar have large molecular weight with abundant functional groups, high-precision numerical basis set could reduce the superposition error of basis sets and accurate description. Therefore, the Zn-BTC@SBC models with different oxygen-containing functional groups and TC molecules were geometrically optimized by Gaussian 09 package using 6-31G (d, p) (liquid phase) standard basis set basis [37]. In order to visualize biochar, six aromatic rings structures were simulated the structure of Zn-BTC@SBC. The software Multiwfn 3.6 and VMD 1.9.3 for theoretical calculations of electrostatic potential [38] and frontier electron orbitals [39]. The microscopic interaction structure between TC and Zn-BTC@SBC was studied by spin polarization DFT simulation using the Dmol3 package in Materials Studio 2017. The k-points were set to $8 \times 8 \times 1$ for structure and establish a vacuum distance perpendicular to the plane of 15 Å. The optimized TC and Zn-BTC@SBC were used to calculate the adsorption energy and adsorption energy (E_{ads}) was calculated as follows:

$$E_{ads} = E_{ad/sub} - (E_{ad} + E_{sub})$$

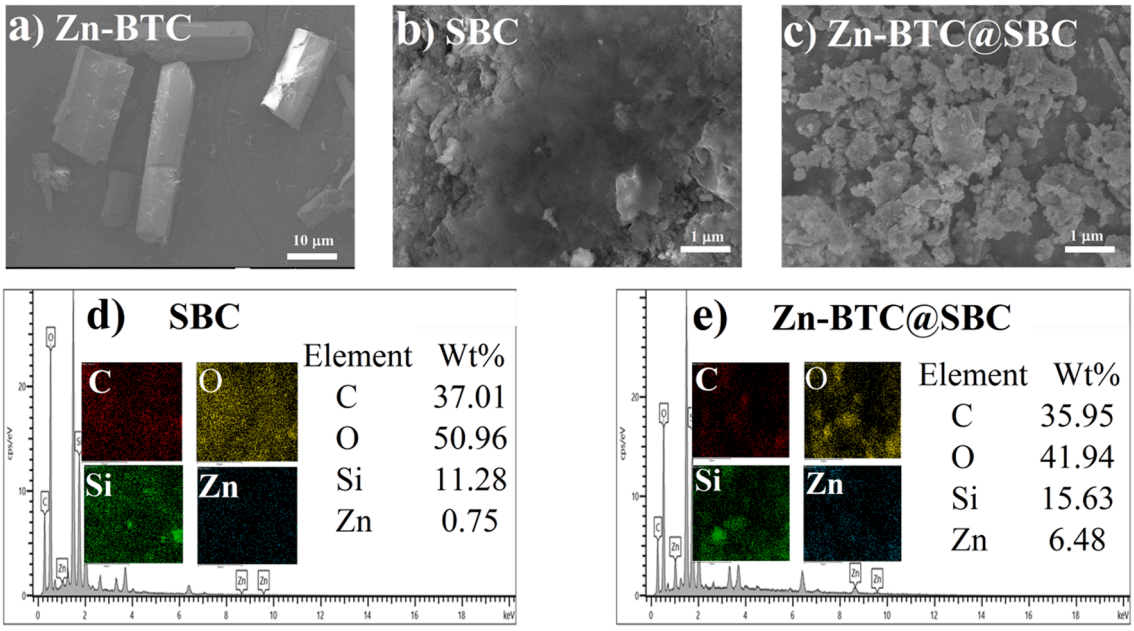

Fig. 1. Surface morphology and elemental mapping of Zn-BTC (a), SBC (b and d), Zn-BTC@SBC (c and e).

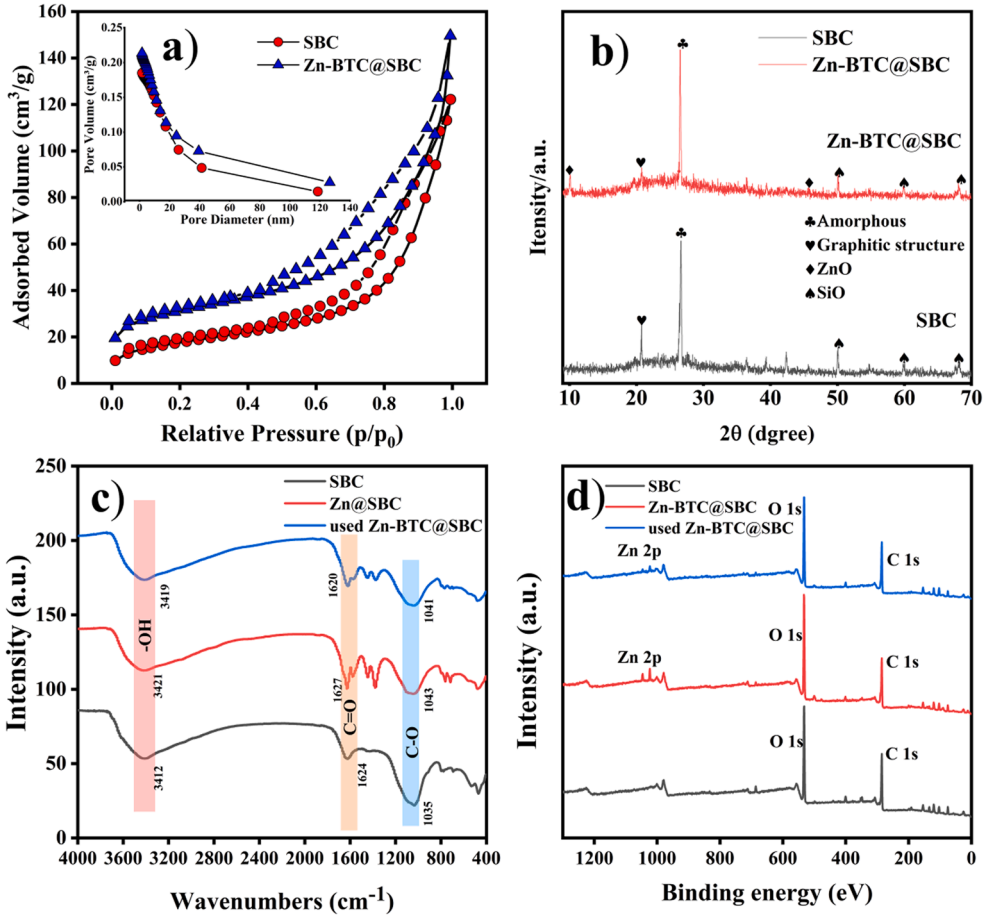

Fig. 2. N_2 adsorption/desorption isotherms and pore diameter distribution of SBC and Zn-BTC@SBC (a); XRD patterns of SBC and Zn-BTC@SBC (b); FTIR spectra (c) and XPS survey spectra (d) of SBC, Zn-BTC@SBC and Zn-BTC@SBC.

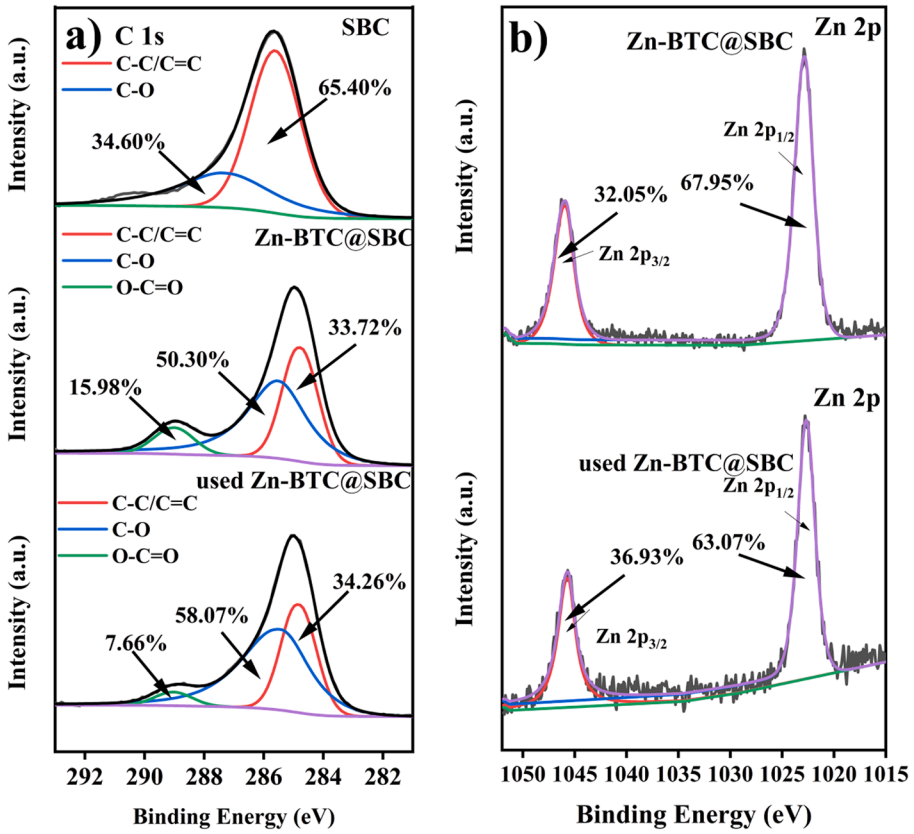

Fig. 3. The XPS spectra of SBC and Zn-BTC@SBC composite: high resolution XPS spectrum of C 1 s (a), and Zn 2p (b).

$E_{ad/sub}$, E_{ad}, and E_{sub} were the total energies of Zn-BTC@SBC after adsorption of TC, the energy of Zn-BTC@SBC, and the energy of optimized TC, respectively.

3. Results and discussion

3.1. Characterization

Clearly, Zn-BTC exhibited the typical hexagonal prism structure (Fig. 1(a)) and Zn was adhered on the surface of SBC, which showed agglomerated shape morphological structure or snowflake shape (Fig. 1 (c)). The SBC surface was smooth, with no apparent holes, as seen in Fig. 1b, while Zn-BTC@SBC surface was rough and heterogeneous, developing large amounts of irregular cracks or cavities (Fig. 1(c)). The rough and heterogeneous surface of Zn-BTC@SBC guaranteed its superior porous structure. These results might be attributed to that Zn could break the organic matter in SBC, then recombined the solid matrix in the high temperature to develop more porous structures [40]. The elemental mapping analysis (Fig. (d and e)) showed that C, O and Si elements were uniformly distributed in SBC and Zn-BTC@SBC. Notably, Zn-BTC@SBC had a significantly higher Zn content (6.48 %) than that of SBC (0.75 %), illustrating that Zn-BTC was successfully loaded onto its surface.

The porous structure of the biochar surface facilitated the adsorption of target pollutants [41]. To further investigate the physical structure of SBC and Zn-BTC@SBC, N_2 adsorption–desorption isotherms were carried out and pore structure were analyzed by BET (Fig. 2(a)). The results have showed Zn-BTC@SBC had the larger surface area and pore volume. The pore size distribution indicated that SBC and Zn-BTC@SBC possessed the similar pore size distribution. After SBC was loaded by Zn-BTC, BET surface areas (S_{BET}) and total pore volume (V_t) grew by1.75 and 1.15 times (Table. S1). The larger surface area and pore volume were capable of providing more active sites for TC adsorption [23,30]. This might be assigned to that the alkaline metal of Zn in Zn-BTC could act as an activation agent for pore development during the pyrolysis process of SBC through dehydrogenation and deoxygenation [40,42].

The distribution of functional groups on biochar surfaces played crucial roles in the adsorption of TC [30].The surface functional groups of SBC and Zn-BTC@SBC were analyzed by FTIR (Fig. 2(c)). The peaks located at 3420–3445 cm^{-1} corresponded to the stretching vibration of –OH derived from intermolecular hydrogen in alcohol and phenol [22]. The absorption peaks appeared at 1577–1625 cm^{-1} and 1083–1091 cm^{-1}, which were related to C═O and C—O, respectively [22]. There were more oxygen-containing functional groups (such as C═O and –OH) on the surface of Zn-BTC@SBC compared to SBC, which might be attributed to the Zn-BTC supporting [43]. As previous studies pointed out, zinc chloride could mutually transform the oxygen-containing functional groups on the surface of biochar at high temperature to achieve a reasonable distribution, and thus enhancing the adsorption performance [44]. On the other hand, metal zinc dehydrated during carbonization to form zinc oxide, which was fixed on the surface of biochar to reduce the loss of oxygen [45]. Yan et al (2020) reported that these oxygen-containing functional groups on the biochar surface acted as π-electron acceptors and the special benzene (four aromatic rings) ring structure of TC acted as π-electron donors, which strengthened the π-π conjugation between Zn-BTC@SBC and TC [30]. Additionally, the H-bonding between the –OH of TC and the –OH on Zn-BTC@SBC surface was also favorable for TC adsorption [46]. As shown in Fig. 3a, the bending vibration of –OH, C═O and C—O shifted marginally to the lower wave numbers after TC adsorption, manifesting that surface complexation, H-bonding and π-π interaction jointly contributed to TC removal [47]. In previous studies found that TC molecules and biochar with oxygen-containing functional groups could easily form a π-electron donor-electron acceptor system duo to phenol, amine, hydroxyl and enone moieties in TC molecules, especially enone structure, which could form H-bonding and π-π interaction [30,48].

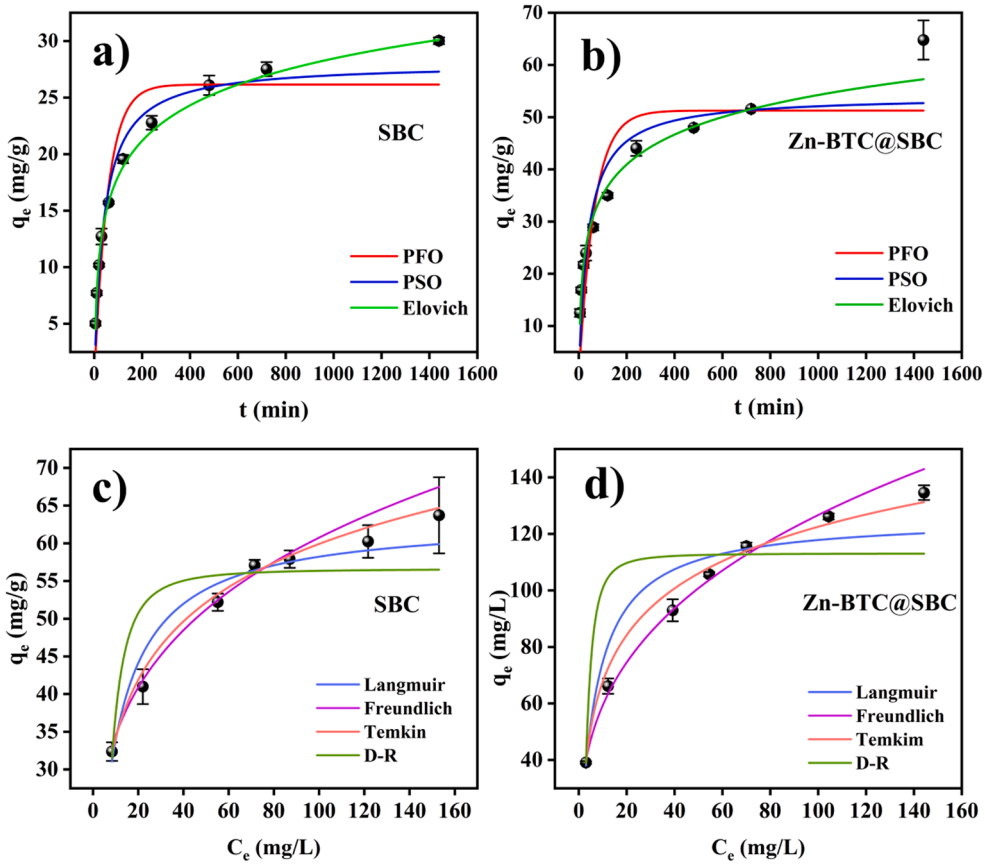

Fig. 4. Adsorption kinetics of SBC (a) and Zn-BTC@SBC (b).Conditions: C_0 (TC) = 20 mg/L, V = 0.1 L, m = 0.04 g, T = 298 K, and t = 0–1440 min; adsorption isotherm of SBC (c) and Zn-BTC@SBC (d). Conditions: C_0 (TC) = 10–150 mg/L, m = 0.04 g, V = 0.1 L, T = 298 K, and t = 0–1440 min.

Fig. 2(b) showed the XRD pattern of SBC and Zn-BTC@SBC. The sharp characteristic peaks around 2θ = 26° were defined as the amorphous carbon, implying the formation of graphite crystals in disordered carbon [49]. Graphitic structures could act as π-donor and promote the behavior of pollutant adsorption [15]. The result consisted with the Raman spectra (Fig.S1). The lower value of I_D/I_G (I_D/I_G = 0.9) of Zn-BTC@SBC implied its greater graphite degree than that of SBC (I_D/I_G = 1.1) [50]. The greater graphite degree enhanced the π-π conjugation between Zn-BTC@SBC and TC. Two new peaks appearing at 2θ = 10°and 2θ = 47.6° were related to the generation of ZnO (JCPDS standard card 51–1525).

The XPS spectrum illustrated the chemical composition of SBC, Zn-BTC@SBC and Zn-BTC@SBC after adsorption (used Zn-BTC@SBC). As shown in Fig. 2(d), they had common characteristic peaks of C 1 s and O 1 s at 284.8 eV and 532.0 eV, respectively. Additionally, new peaks appeared around 1021 eV and 1044 eV on Zn-BTC@SBC and used Zn-BTC@SBC corresponded to Zn 2p [51]. The appearance of Zn 2p on Zn-BTC@SBC illustrated that Zn-BTC was successfully supported onto its surface. The two fitted peaks of C 1 s (Fig. 3(a)) could be ascribed to C—C/C═C (284.2 eV, 65.4 %) and C—O (286.2 eV, 34.6 %), while the C 1 s spectra of Zn-BTC@SBC could be decomposed into three corresponding peaks of C—C/C═C (284.8 eV, 33.72 %), C—O (285.5 eV, 50.30 %) and O-C═O (289.0 eV, 15.98 %). The C—C/C═C content was decreased and the contents of C—O and O-C═O performed the corresponding increase on Zn-BTC@SBC compared to that of SBC, which demonstrated that Zn-BTC supporting introduce more oxygen-containing functional groups. Compared with Zn-BTC@SBC, the O-C═O on the used Zn-BTC@SBC was decreased, suggesting it participated in the π-π conjugation between Zn-BTC@SBC and TC. To determine the valence state on Zn-BTC@SBC, the core element Zn was further analyzed by high-resolution XPS spectroscopy (Fig. 3(b)). As can be seen, the peaks at about 1021.5 eV and 1044.5 eV were ascribed to $2p_{3/2}$ and $2p_{1/2}$ of Zn^{2+}, respectively. It has reported the Zn $2p_{3/2}$ peak at the binding energy of 1021.5 eV was attributed to zinc oxide [51]. After TC absorption, a decrease was observed in the binding energy values of Zn-BTC@SBC. The result consisted with the previous reports [30,52]. The result was likely due to the complexation interaction of Zn with functional groups (hydroxyl or amino groups) on TC, which resulted in changes in the electron cloud density and a charge shift of Zn-BTC@SBC [52]. For Zn-BTC@SBC, these phenomena all proved that zinc and biochar could be closely combined, not just physical mixing or loading [47].

3.2. Effect of Zn-BTC@SBC dose on TC adsorption

Obviously, the removal rate of TC was increased with the dosage of Zn-BTC@SBC increasing, and the removal rates of TC were 72.55 %, 84.96 %, 92.15 % and 95.17 % at the dose of 0.02 g, 0.03 g, 0.04 g and 0.05 g (t = 1440 min), respectively (Fig. S2). However, the removal efficiencies and rates of TC at the dose of 0.04 g and 0.05 g had no significant difference. Taking into account the combined consideration of low cost and removal rate, a dose of 0.04 g was chosen for subsequent experiments.

3.3. Adsorption kinetics

Clearly, the adsorption capacity of Zn-BTC@SBC for TC depended on the reaction time (Fig. 5 (a)). The whole adsorption process of TC onto Zn-BTC@SBC could be divided into two sections, namely fast adsorption and slow adsorption stages. The fast adsorption occurred in the initial 240 min, which shared about 60 % and 40 % of the equilibrium adsorption amount of TC by Zn-BTC@SBC and SBC, respectively. This

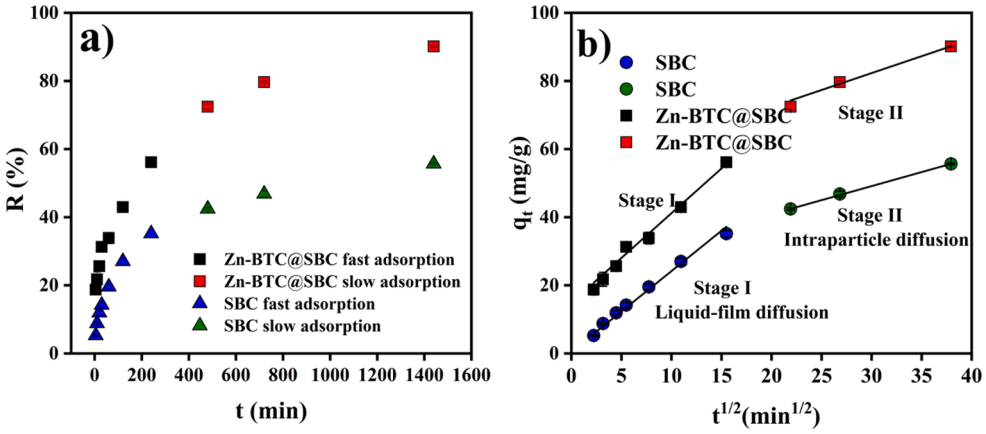

Fig. 5. Effect of contact time on removal rate of TC by SBC and Zn-BTC@SBC (a), intraparticle diffusion (b) fitting of TC adsorption onto SBC and Zn-BTC@SBC. Conditions: C_0 (TC) = 20 mg/L, V = 0.1 L, m = 0.04 g, T = 298 K, and t = 0–1440 min.

Table 1
Pseudo-first-order, Pseudo-second-order and Elovich fitting parameters of TC adsorption onto SBC and Zn-BTC@SBC.

Models Parameters		Biochars SBC	Zn-BTC@SBC
Pseudo-first-order	$Q_{e,cal}$ (mg/g)	26.25	42.09
	k_1 (min^{-1})	0.018	4.000×10^{-3}
	R^2	0.8491	0.8923
Pseudo-second-order	$Q_{e,cal}$ (mg/g)	28.04	44.33
	K_2 (g/mg min)	8.981×10^{-4}	1.000×10^{-3}
	R^2	0.9452	0.9500
Elovich	α (mg/g min)	2.449	6.876
	β (mg/g)	0.2210	0.1490
	R^2	0.9962	0.9981

Table 3
Langmuir, Freundlich, Temkin and D-R isotherms models fitting parameters of TC adsorption onto SBC and Zn-BTC@SBC.

Models	Parameters	Biochars SBC	Zn-BTC@SBC
Langmuir	q_m (mg/g)	63.29	125.9
	K_L (L/mg)	0.1182	0.1463
	R^2	0.8493	0.8925
Freundlich	K_F (L/mg)	19.52	27.78
	n	4.056	3.036
	R^2	0.9826	0.9973
Temkin	K_t	2.088	1.720
	b_t	0.2212	0.1491
	R^2	0.9963	0.9981
D-R	q_m (mg/g)	56.61	113.1
	β (mol^2 KJ^{-2})	7.544×10^{-6}	2.066×10^{-6}
	R^2	0.8923	0.9504

phenomenon was connected with adsorption sites and the mass transfer driving force. A significant number of active sites were not occupied during the early stages. After that, the adsorption process gradually reached equilibrium because the large numbers of TC had occupied the sites, which increased the diffusion resistance of TC adsorbed onto biochar (Fig. 5(a)).

Pseudo-first-order (PFO), pseudo-second-order and Elovich models were used to in this study fit the adsorption kinetics data to investigate the adsorption mechanism of TC onto biochar. The fitting curves and paremeters were shown in Fig. 4 (a and b) and Table 1, respectively. It was well known that, PFO model mainly described a physical adsorption process, while PSO model illustrated a physical adsorption process that reached equilibrium, then switched to chemisorption (including the formation of covalent bonds) [53]. Elovich model described the chemisorption took place between solid and liquid phases [54]. Obviously, The R^2 values of the Elovich model (0.9962–0.9981) were better than that of the PFO model (0.8491–0.8923) and PSO model (0.9452–0.9500), suggesting that chemisorption including electrostatic attraction, π-π conjugation and hydrophobic bond might be involved in the adsorption processes of TC [21,55].

Intraparticle diffusion (IPD) model was also employed to fit the kinetics data to further investigate the adsorption process and main rate-limiting step. As shown in Fig. 5(b), two stages included in IPD model: liquid-film diffusion (stage I) and intraparticle diffusion (stage II). Obviously, these fitting plots did not pass through the origin (the intercepts varied from 0.4693 to 52.52), implying that there were other rate-limiting steps. The adsorption processes of TC onto SBC and Zn-BTC@SBC were simultaneously controlled by both liquid film and intraparticle diffusion. The greater adsorption efficiency in the stage I was ascribed to the abundant available adsorption sites on the surface of adsorbents. After that, their adsorption sites gradually reached saturation in stage I, TC molecule further transferred into the inner pores in stage II. The processes of TC adsorption onto adsorbents (SBC and Zn-BTC@SBC) could be summarized as follows: TC diffused from its bulk solution to the external surface of SBC and Zn-BTC@SBC (stage I), then gradually moved into their inner pores (stage II). The value of C in IPD represented the thickness of boundary layer. Table 2 showed that the C_{II} values of both SBC and Zn-BTC@SBC were greater than the C_I values, indicating a greater diffusion resistance of TC adsorption in stage II. This result might be assigned to that TC molecules have occupied most available active sites in stage I, which increased the diffusion resistance. These behaviors have also been described in the previous studies of tetracycline and ciprofloxacin adsorption to Fe/Zn-SBC and tetracycline adsorption onto MoS_2@SBC [21,22].

Table 2
Intraparticle diffusion fitting parameters of TC adsorption onto SBC and Zn-BTC@SBC.

Biochars	Liquid-film diffusion (0–240 min)				Intraparticle diffusion (240–1440 min)	
	K_I(mg/g min$^{1/2}$)	C_I	R_I^2	K_{II}(mg/g min$^{1/2}$)	C_{II}	R_{II}^2
SBC	2.373	0.4691	0.9843	0.8235	24.41	0.9992
Zn-BTC@SBC	2.624	14.90	0.9847	0.9923	55.52	0.9994

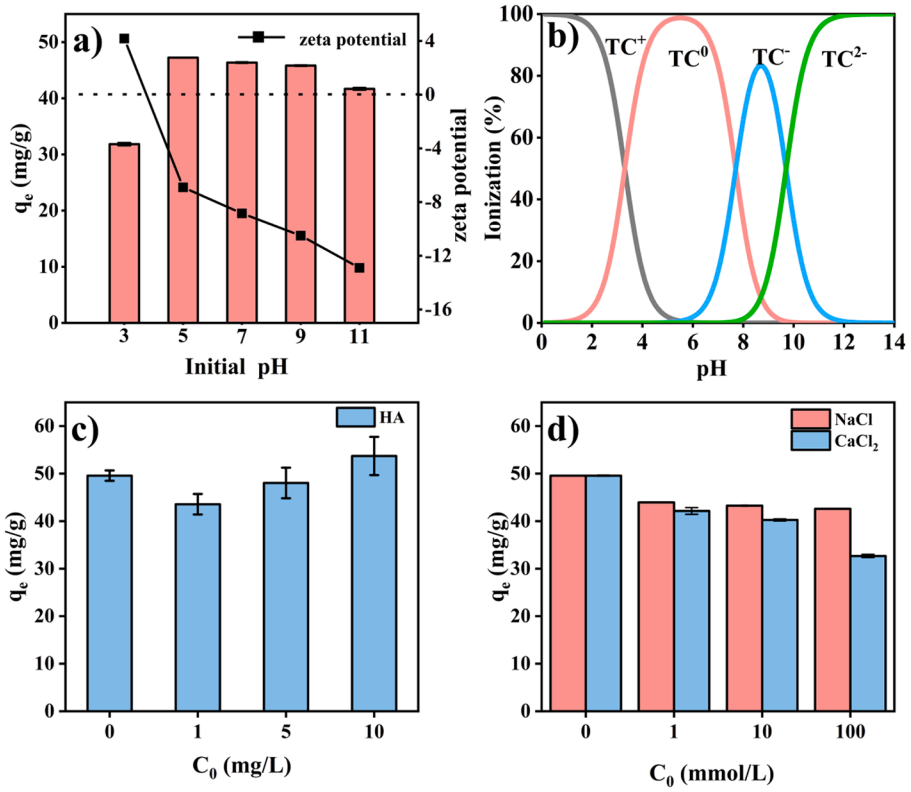

Fig. 6. Effect of initial pH on adsorption capacity of Zn-BTC@SBC for TC, zeta potential of Zn-BTC@SBC (a) and species of TC distribution (b); effect of ion species/strength (c) and humic acid concentration on adsorption capacity of Zn-BTC@SBC for TC (d). Conditions: C_0 (TC) = 20 mg/L, V = 0.1 L, m = 0.04 g, pH = 3–11, HA = 0–10 mg/L, C_0 (NaCl or $CaCl_2$) = 1–100 mM, T = 298 K, and t = 0–1440 min.

3.4. Adsorption isotherms and thermodynamics

Isotherms are the primary tool for describing and predicting the mobility of substances in the environment as they move from the mobile phase (liquid or gas) to the solid phase. Langmuir, Freundlich, Temkin and Dubinin–Radushkevich (D-R) isotherm models were applied to fit the isotherms data (Table 3). Langmuir model assumed that it was a monolayer chemical adsorption occurred on the homogeneous surface of adsorbent. Generally, it was used to assess the maximum adsorption capacity of adsorbent [56]. The maximum adsorption capacity of SBC and Zn-BTC@SBC were 63.29 mg/g and 125.9 mg/g according to Langmuir model, respectively. The maximum adsorption capacity of Zn-BTC@SBC synthesized in this study for TC was 1.99 times that of SBC, also it was greater than those of 51.78 mg/g [57] and 93.44 mg/g [30]. Freundlich model described a multilayer physical adsorption and the adsorption surface was heterogeneous [47]. The affinity coefficient of (K_F (L/mg)) Freundlich could also reflect the adsorption performance of biochar [17]. Additionally, the adsorption process was considered to be favorable when the value of 1/n was less than 0.5 [57]. The values of 1/n were 0.24 (SBC) and 0.32 (Zn-BTC@SBC), demonstrating that the adsorption processes of TC onto SBC and Zn-BTC@SBC were favorable. Temkin model described the relationship between adsorption energy and surface coverage which illustrated the chemisorption process [22]. The R^2 values of Temkin model fitting suggested that chemisorption and strong intermolecular forces played a key role in the adsorption process of TC [58]. Additionally, the high correlation coefficient of Freundlich model fitting appeared in both SBC and Zn-BTC@SBC (R^2 = 0.982–0.997), which suggested that physical interactions (e.g., pore filling) might also involve in their adsorption process. Generally, the mean free energy ($E\,(kJ/mol) = 1/\sqrt{2\beta}$) could be used to identify whether the adsorption process of TC was chemical or physical [21]. The E value was less than 8 kJ/mol calculated from D-R model, which illustrated that chemisorption was the major adsorption mechanism of TC adsorption onto Zn-BTC@SBC.

To understand the thermodynamic properties of TC adsorption onto Zn-BTC@SBC, adsorption experiments were carried out at different temperatures (Fig S3). A temperature rise was beneficial for TC adsorption, which reflected that adsorption was an endothermic process. Obviously, the adsorption capacity of Zn-BTC@SBC was increased with reaction temperature increasing (Fig. S3). The thermodynamics parameters of $\Delta H > 0$ in Table. S2 further confirmed above results [22]. All ΔG values were negative and dropped as the temperature increased with the reaction temperature, implying TC adsorption by Zn-BTC@SBC was spontaneous and the driving force for adsorption was steadily promoted. ΔS described the randomness and affinity of the solid-solution interface [21]. The positive ΔS value demonstrated the higher reaction temperature improved the randomness of solid–liquid interfaces. Briefly, the process of TC adsorption onto Zn-BTC@SBC was a spontaneous, endothermic and randomness increasing process.

3.5. Effect of solution pH on TC adsorption

TC was a typical hydrophilic amphiphilic molecule with different acid dissociation constants [59].Solution pH could simultaneously decide the surface charge of adsorbent and species of TC. Fig. 6(b) described that TC were mainly forms in different pH [30]. Relevant calculation formulas have been supplemented in supplementary materials (Text S3). The zeta potential of Zn-BTC@SBC decreased dramatically as pH was promoted, and its zero potential charge (pH_{ZPC} = 4.3) (Fig. 6(a)). Fig. 6(a) showed that the maximum adsorption capacity of Zn-BTC@SBC occurred at pH = 5, and it was primarily related to the speciation of TC and surface charge of Zn-BTC@SBC. The same phenomenon was observed on MoS_2-modified SBC, and the adsorption capacity was also maximum at the same pH [21]. This might be attributed

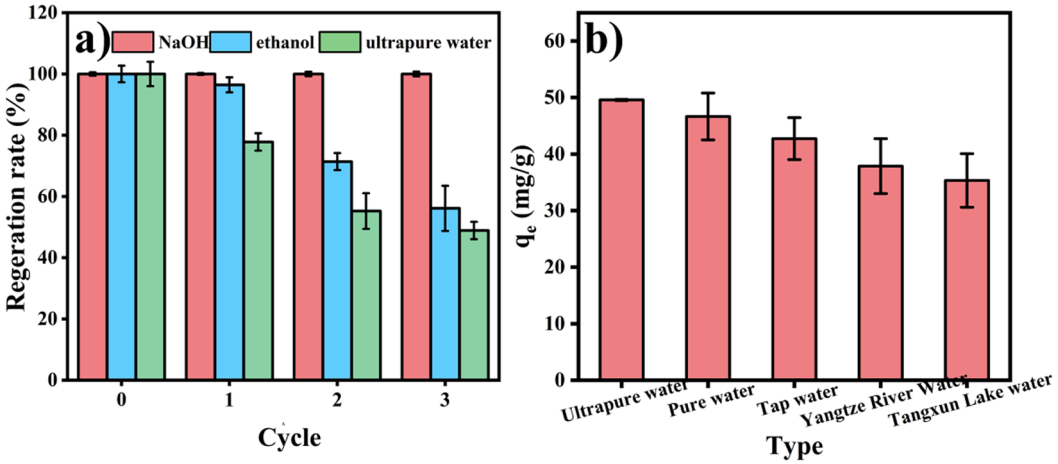

Fig. 7. Regeneration of Zn-BTC@SBC by NaOH, ultrapure water and ethanol treatment in recycles (a) (n = 3). Conditions: C_0 (TC) = 20 mg/L, V = 0.1 L, m = 0.2 g, T = 298 K, and t = 0–1440 min; the adsorption capacity of TC by Zn-BTC@SBC in different water samples (b). Conditions: C_0 (TC) = 20 mg/L, V = 0.1 L, m = 0.04 g, T = 298 K, and t = 0–1440 min.

to that the neutral species of TC were the main chemical forms of TC at pH = 5 and Zn-BTC@SBC surface shifted from positive to negative, which resulted in the weaker electrostatic repulsion between TC and Zn-BTC@SBC.

3.6. Effects of ionic species/strength and HA concentrations

Different inorganic ions were widely present in nature, hence it was necessary to investigate the effect of ionic species/strength on adsorption performance of Zn-BTC@SBC. By adjusting the concentration, the influence of inorganic ions (NaCl and $CaCl_2$) on the adsorption process was investigated (Fig. 6(d)). As showed in Fig. 6(d), the adsorption capacity of Zn-BTC@SBC for TC was decreased in the presence of NaCl and $CaCl_2$, and the inhibitory strength was enhanced with their concentration increasing. This might be assigned to that the presence of NaCl and $CaCl_2$ could eliminate the electrostatic repulsion between Zn-BTC@SBC which caused the aggregation effect. The aggregation of Zn-BTC@SBC would cover their active sites, which was unfavorable for TC adsorption. Particularly, when the concentration of $CaCl_2$ was promoted to 100 mM, the adsorption capacity of Zn-BTC@SBC fell from 49.78 mg/ g to 35.88 mg/g. This was due to the fact that Ca^{2+} could combine with TC to produce Ca-TC compounds, which reduced the affinity of Zn-BTC@SBC for TC.

In natural waters, the decomposition of organic matter produced large amounts of HA, which could have an effect on the adsorption of TC [21]. The effect of HA concentrations (1–10 mg/L) on the adsorption capacity of Zn-BTC@SBC was presented in Fig. 6(c). Notably, the presence of 1 mg/L and 5 mg/L HA were unfavorable for TC adsorption onto Zn-BTC@SBC, while 10 mg/L of HA facilitated TC adsorption. These results were attributed to that the low concentrations of HA could occupy part of the active site on Zn-BTC@SBC, while the high concentration of HA could interact with TC through complexation reaction duo

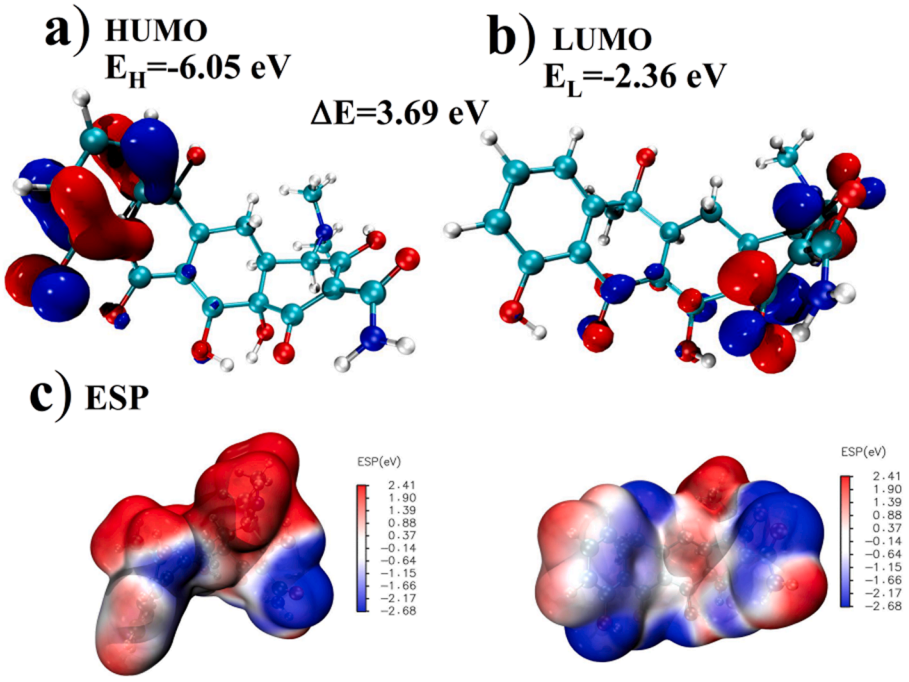

Fig. 8. TC molecule frontier molecular orbital distributions HOMO (a); TC molecule frontier molecular orbital distributions LUMO (b); Electrostatic potential diagrams of TC molecule (c).

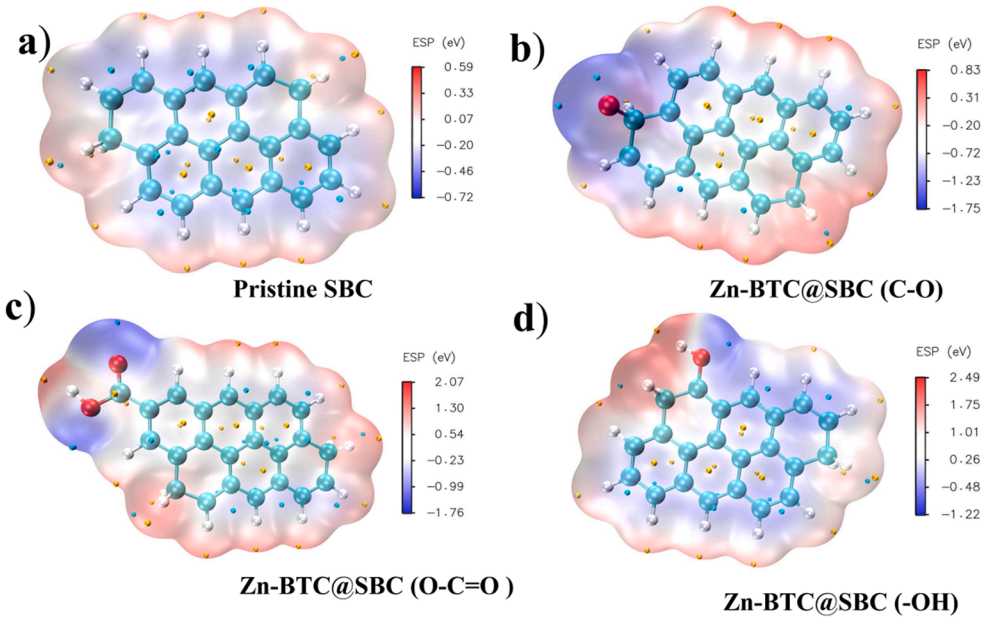

Fig. 9. Electrostatic potential diagram of biochar with different oxygen-containing functional groups.

to hydroxyl groups on the surface of HA molecules, thus assisting Zn-BTC@SBC to improve the removal effect of TC [60].

3.7. Regeneration and real water adsorption

The reusability of adsorbent was a critical indicator to assess its practical application. Ultrapure water, ethanol, and (0.1 mol/L) NaOH were employed to regenerate the used Zn-BTC@SBC. According to Fig. 7 (a), NaOH exhibited the most efficient regeneration effect, followed by ethanol and Ultrapure water. Because NaOH could destroy the physicochemical forces between antibiotics and biochar, break the adsorption equilibrium, desorb the adsorbate from the adsorbent, and realize the efficient regeneration of biochar [61]. After three reuse cycles, the adsorption capacity of the used Zn-BTC@SBC was decreased. While the Zn-BTC@SBC regenerated by NaOH could maintain a stable and efficient adsorption performance for TC after three reuse cycles (98 % of the fresh one).As shown in Fig. S6, even after 10 cycles of regeneration using NaOH, the adsorption performance for TC still maintained 53.39 mg/g (85.81 % of the fresh one). The outstanding regeneration performance by NaOH suggested that it could be used to regenerate the used Zn-BTC@SBC.

The actual water including pure water, tap water, Tangxun Lake water and Yangtze River water were also conducted in this study to evaluate the practical application of Zn-BTC@SBC. The parameters of actual waters were listed in Table S3. As showed in Fig. 7 (b), except ultrapure water, the adsorption capacity of Zn-BTC@SBC for TC were decreased in the other four types of actual water. Specially, the slightly inhibitory effects were observed in Tangxun Lake water and Yangtze River water. This might be due to the considerable amount of inorganic and organic substances contributed to the substantial drop in TC adsorption.

3.8. Adsorption mechanisms and theoretical calculations

The main adsorption mechanism of Zn-BTC@SBC for TC adsorption process of Zn-BTC@SBC on TC involved physicochemical interactions. The superior porous structure (SEM and BET analysis) of Zn-BTC@SBC including larger surface area and pore volume suggested that pore filling was the main physical interaction. The effect of pH illustrated that electrostatic interaction also participated in TC adsorption. The more oxygen-containing functional groups (e.g., O-C═O/C—O and –OH) could enhance the π-π conjugation and H-bonding between Zn-BTC@SBC and TC. Additionally, the greater graphite degree also facilitated the π-π conjugation. The thermodynamics analysis suggested that the process of TC adsorption onto Zn-BTC@SBC was spontaneous, endothermic and randomness increasing.

To further verify the above conclusions more clearly, the molecular structure of TC and the planar binding energy of different oxygen-containing functional groups of biochar were simulated using DFT calculations [62]. Molecules frontier molecular orbital distributions (HOMO- LUMO) and molecular van der Waals (vdW) surface maps for electrostatic potential energy coloring for TC were analyzed [38]. All the isomers of TC and Zn-BTC@SBC with oxygen-containing functional groups and their energies showed in the supplementary material (Fig. S4). The study of HOMO and LUMO molecular orbitals was important because the chemisorption properties could be understood at the molecular level. In addition, HOMO and LUMO molecular orbital energies reflected the ability of the molecular to donate and receive electrons [63]. As shown in Fig. 8, the HOMO and LUMO orbitals were mainly distributed in the benzene ring on both sides of TC, where the *N*-functional group rich benzene ring contained lone pairs of electrons more likely to form sp^2 conjugated systems through π-π conjugation [64]. Also, quantum mechanical calculations yielded values of −6.05 eV and −2.36 eV for E_H and E_L, respectively, with an energy gap of 3.69 eV. The small energy gap between HOMO- LUMO indicated that TC was polarized and had strong chemical properties (π-π conjugation, H-bonding and electrostatic interaction) for the adsorbed TC on the adsorbents surface [63]. As the previous FTIR and XPS analysis chemical properties results remained consistent. As shown in Fig. 8c, ESP mapped molecular vdW surface of TC, where red represented high electron density and blue represented low electron density. The presence of *N*-containing functional groups greatly enriched the electron density, and the maximum electron density reached 2.31 eV. The rich electron density of TC could form aromatic rings well with adsorbent surface through π-π EDA interaction [37]. In general, TC molecules could also act as both hydrogen bond donors and acceptors, facilitating interactions with many oxygen-containing functional groups on the surface of adsorbent. The FTIR and XPS results (Fig. 2(c) and (d)) have revealed that the functional groups on the Zn-BTC@SBC surface were changed both before and after TC adsorption, which had a direct effect on the

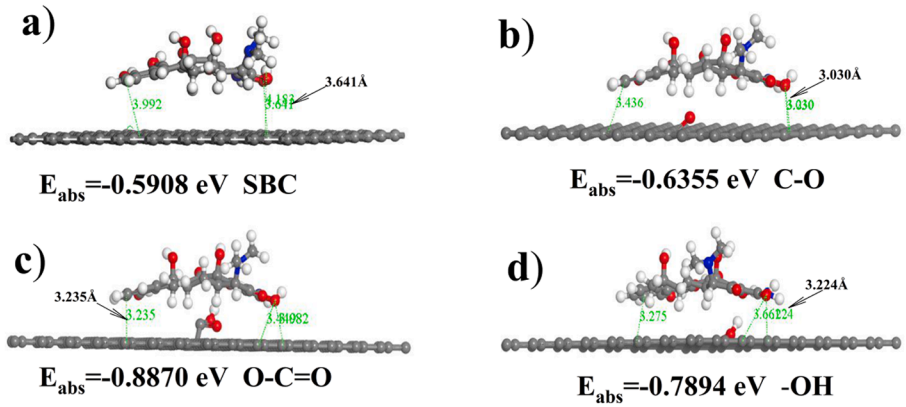

Fig. 10. Adsorption equilibrium configurations and adsorption energies of TC on biochar with different oxygen-containing functional groups.

adsorption. Compared with the pristine SBC, the involvement of oxygen-containing functional groups greatly enriched the distribution of electrons on the surface of Zn-BTC@SBC (Fig. 9). The yellow ball represented the point of maximum electrostatic potential and the green ball represented the point of minimum electrostatic potential. Certainly, different oxygen-containing functional groups contributed differently to the electron density of the Zn-BTC@SBC surface. Among the oxygen-containing functional groups, the introduction of C—O (-1.747 eV) and O-C═O (-1.762 eV) could significantly reduce the surface electron density of Zn-BTC@SBC (green ball) and promote the formation of π-π conjugation between Zn-BTC@SBC and TC. On the contrary, the presence of –OH functional groups enriched the electron density on the Zn-BTC@SBC surface (yellow ball) (Fig. 9(d)), which indicated that more lone pairs of electrons were provided [64]. Then lone pairs of electrons facilitated electrophilic interactions with the hydroxyl groups on the TC (blue part) to form hydrogen bonds [37]. Not only that, the introduction of oxygen-containing functional groups on biochar (Fig. 9) changed the extreme point and electrostatic potential of the surface, mainly by affecting the density of electrons on the surface of the biochar.

Combined above results, the adsorption equilibrium configuration and adsorption energy of TC on Zn-BTC@SBC were also studied in this study. In order to simplify the calculation model, the structure of graphene was simulated as biochar. Different equilibrium configurations of TC and biochar were calculated and shown in Fig. S7.The lowest adsorption energy was selected as the research object of equilibrium configuration. As the results of calculation, the adsorption energy of pristine SBC (Fig. 10(a)) was lower than that of Zn-BTC@SBC containing oxygen functional groups. The corresponding adsorption energies of different oxygen-containing functional groups were as follows: $E_{abs,O-C\_O}$ = -0.8870 eV > $E_{abs,-OH}$ = -0.7894 eV > $E_{abs,C—O}$ = -0.6355 eV > $E_{abs,SBC}$ = -0.5874 eV. Therefore, the above results suggested that improving the oxygen-containing functional groups of biochar could significantly improve adsorption capacity for TC. Additionally, compared to the SBC, significant changes in distances were observed between TC surface and Zn-BTC@SBC surface, in which the distances values ranged decreased from 3.641 Å to 3.030 Å (C—O), 3.235 Å (O-C═O) and 3.224 Å (–OH), respectively. The above results indicated a strong affinity between the oxygen-containing functional groups and TC.

4. Conclusions

Zinc metal organic framework porous biochar composite of Zn-BTC@SBC was synthesized and showed superior porous structure, greater graphite degree and more oxygen-containing functional groups. The characterization of Zn-BTC@SBC and correlation analysis demonstrated that pore filling, π-π conjugation, H-bonding and electrostatic interaction were all essential driving forces for promoting TC adsorption on Zn-BTC@SBC. The characterization results and DFT calculations demonstrated that TC molecules could be adsorbed by forming chemical bonds with the oxygen-containing functional groups on the Zn-BTC@SBC surface. Elovich and Temkin models better fitted the kinetics and isotherms data illustrated that chemical forces were the dominant mechanism. Solution pH, ionic species/strength and HA concentrations were demonstrated to be the environmental factors affecting the adsorption performance of Zn-BTC@SBC. The process of TC adsorption onto Zn-BTC@SBC involved mainly spontaneous, endothermic and randomness increasing. NaOH could effectively regenerate the used Zn-BTC@SBC. The adsorption capacity of Zn-BTC@SBC for TC in natural water (lake and river water) still remained at 71.27–76.37 %. The outstanding adsorption performance of Zn-BTC@SBC enabled it to be a promising adsorbent for TC elimination.

CRediT authorship contribution statement

Zhikang Deng: Conceptualization, Writing – review & editing. **Jinyao Zhu:** Conceptualization, Writing – review & editing. **Ping Li:** Data curation, Writing – review & editing. **Zhenjie Du:** Data curation, Writing – review & editing. **Xuebin Qi:** Data curation, Writing – review & editing. **Xi Chen:** Methodology, Conceptualization. **Rui Mu:** Methodology, Conceptualization. **Chenyu Zeng:** Methodology, Conceptualization. **Yongfei Ma:** Supervision, Conceptualization, Writing – review & editing. **Zulin Zhang:** Supervision, Conceptualization, Writing – review & editing.

Declaration of Competing Interest

The authors declare that they have no known competing financial interests or personal relationships that could have appeared to influence the work reported in this paper.

Data availability

The authors do not have permission to share data.

Acknowledgements

This work was supported by the National Natural Science Foundation of China (No. 52170171) and the Scottish Government's Rural and Environment Science and Analytical Services Division (RESAS).

Appendix A. Supplementary data

Supplementary data to this article can be found online at https://doi.org/10.1016/j.molliq.2023.122283.

References

[1] Q.Q. Zhang, G.G. Ying, C.G. Pan, Y.S. Liu, J.L. Zhao, Environ. Sci. Tech. 49 (2015) 6772.
[2] L. Xu, H. Zhang, P. Xiong, Q. Zhu, C. Liao, G. Jiang, Sci. Total Environ. 753 (2021), 141975.
[3] J.E. Kim, S.K. Bhatia, H.J. Song, E. Yoo, H.J. Jeon, J.-Y. Yoon, Y. Yang, R. Gurav, Y.-H. Yang, H.J. Kim, Y.-K. Choi, Bioresour. Technol. 306 (2020), 123092.
[4] V. Frišták, M. Pipíška, M. Hubeňák, M. Kadlečíková, M. Galamboš, G. Soja, Water, Air, Soil Pollut. 229 (2018) 146.
[5] A.M. Botero-Coy, D. Martinez-Pachon, C. Boix, R.J. Rincon, N. Castillo, L.P. Arias-Marin, L. Manrique-Losada, R. Torres-Palma, A. Moncayo-Lasso, F. Hernandez, Sci. Total Environ. 642 (2018) 842.
[6] Y. Xiang, Z. Xu, Y. Wei, Y. Zhou, X. Yang, Y. Yang, J. Yang, J. Zhang, L. Luo, Z. Zhou, J. Environ. Manage. 237 (2019) 128.
[7] L. Lai, Q. Xie, L. Chi, W. Gu, D. Wu, J. Colloid Interface Sci. 465 (2016) 76.
[8] Y. Hu, L. Jiang, T. Zhang, L. Jin, Q. Han, D. Zhang, K. Lin, C. Cui, J. Hazard. Mater. 360 (2018) 364.
[9] L. Yue, S. Wang, G. Shan, W. Wu, L. Qiang, L. Zhu, Appl Catal B 176–177 (2015) 11.
[10] M. Jafari, A.A. Abdollahzadeh, F. Aghababaei, Mine Water Environ. 36 (2016) 323.
[11] X. Yang, R.C. Flowers, H.S. Weinberg, P.C. Singer, Water Res. 45 (2011) 5218.
[12] W. Liu, W. Huang, Z. Cao, Y. Ji, D. Liu, W. Huang, Y. Zhu, Z. Lei, J. Hazard. Mater. 438 (2022), 129286.
[13] C. Liang, Y. Tang, X. Zhang, H. Chai, Y. Huang, P. Feng, Environ. Res. 182 (2020), 109059.
[14] Q. Liu, L.B. Zhong, Q.B. Zhao, C. Frear, Y.M. Zheng, ACS Appl. Mater. Interfaces 7 (2015) 14573.
[15] Y. Ma, S. Chen, Y. Qi, L. Yang, L. Wu, L. He, P. Li, X. Qi, F. Gao, Y. Ding, Z. Zhang, Chemosphere (2021), 132707.
[16] J. Qu, X. Dai, H.-Y. Hu, X. Huang, Z. Chen, T. Li, Y. Cao, G.T. Daigger, ACS ES&T Engineering 2 (2022) 323.
[17] Y. Xiang, H. Zhang, S. Yu, J. Ni, R. Wei, W. Chen, Bioresour. Technol. 360 (2022), 127647.
[18] B.M. Cieślik, J. Namieśnik, P. Konieczka, J. Clean. Prod. 90 (2015) 1.
[19] N. Tripathi, C.D. Hills, R.S. Singh, C.J. Atkinson, npj Climate and Atmospheric Science 2 (2019).
[20] M.A. Al-Ghouti, M. Khan, M.S. Nasser, K. Al-Saad, O.E. Heng, Environ. Technol. Innov. 21 (2021), 101267.
[21] J. Zhu, Y. Ma, X. Chen, J. Tang, L. Yang, Z. Zhang, J. Water Process Eng. 49 (2022).
[22] Y. Ma, L. Wu, P. Li, L. Yang, L. He, S. Chen, Y. Yang, F. Gao, X. Qi, Z. Zhang, J. Hazard. Mater. 407 (2021), 124777.
[23] D. Wei, H.H. Ngo, W. Guo, W. Xu, B. Du, M.S. Khan, Q. Wei, Bioresour. Technol. 249 (2018) 410.
[24] T. Chen, L. Luo, S. Deng, G. Shi, S. Zhang, Y. Zhang, O. Deng, L. Wang, J. Zhang, L. Wei, Bioresour. Technol. 267 (2018) 431.
[25] Y. Ma, T. Lu, J. Tang, P. Li, O. Mašek, L. Yang, L. Wu, L. He, Y. Ding, F. Gao, X. Qi, Z. Zhang, Sep. Purif. Technol. 297 (2022), 121426.
[26] J. Zhang, J. Shao, X. Zhang, G. Rao, G. Li, H. Yang, S. Zhang, H. Chen, Chem. Eng. J. 452 (2023).
[27] F. Xu, S. Xian, Q. Xia, Y. Li, Z. Li, Adsorpt. Sci. Technol. 31 (2013) 325.
[28] C. Li, F. Wang, X. Xu, Y. Shi, J. Liang, R. Yang, J. Liu, Z. Zhao, Chem. Eng. J. (2022).
[29] D. Angın, E. Altintig, T.E. Köse, Bioresour. Technol. 148 (2013) 542.
[30] L. Yan, Y. Liu, Y. Zhang, S. Liu, C. Wang, W. Chen, C. Liu, Z. Chen, Y. Zhang, Bioresour. Technol. 297 (2020), 122381.
[31] K. Wang, J. Shu, V.K. Sharma, C. Liu, X. Xu, N. Nesnas, H. Wang, Sci. Total Environ. 805 (2022).
[32] R. Gokulan, A. Avinash, G.G. Prabhu, J. Jegan, J. Environ. Chem. Eng. 7 (2019), 103297.
[33] Y. Shen, N. Zhang, Bioresour. Technol. 282 (2019) 294.
[34] Z. Jin, B. Wang, L. Ma, P. Fu, L. Xie, X. Jiang, W. Jiang, Chem. Eng. J. 385 (2020), 123843.
[35] J. Zhu, Y. Ma, X. Chen, J. Tang, L. Yang, Z. Zhang, J. Water Process Eng. 49 (2022), 103089.
[36] D.A. Thompson, H.J. Lehmler, D.W. Kolpin, M.L. Hladik, J.D. Vargo, K.E. Schilling, G.H. LeFevre, T.L. Peeples, M.C. Poch, L.E. LaDuca, D.M. Cwiertny, R.W. Field, Environ Sci Process Impacts 22 (2020) 1315.
[37] H. Cheng, H. He, Z. Zhang, K. Xiao, Y. Liu, X. Kang, X. Li, Sep. Purif. Technol. 303 (2022).
[38] S. Sánchez, M.E. Martínez, M.T. Espejo, R. Pacheco, F. Espinola, G. Hodaifa 13 (2001).
[39] T. Lu, F. Chen, J. Comput. Chem. 33 (2012) 580.
[40] X. Yang, W. Wang, S. Feng, L. Jin, T.J. Lu, Y. Chai, Q. Zhang, Energy Procedia 88 (2016) 566.
[41] L. Wang, Y. Wang, F. Ma, V. Tankpa, S. Bai, X. Guo, X. Wang, Sci. Total Environ. 668 (2019) 1298.
[42] I. Ihsanullah, M.T. Khan, M. Zubair, M. Bilal, M. Sajid, Chemosphere 289 (2022), 133196.
[43] Q. Liu, S. Jiang, X. Su, X. Zhang, W. Cao, Y. Xu, Chemosphere 275 (2021), 129966.
[44] P.S. Thue, D.R. Lima, E.C. Lima, R.A. Teixeira, G.S. dos Reis, S.L.P. Dias, F. M. Machado, J. Environ. Chem. Eng. 10 (2022).
[45] P.S. Thue, E.C. Lima, J.M. Sieliechi, C. Saucier, S.L.P. Dias, J.C.P. Vaghetti, F. S. Rodembusch, F.A. Pavan, J. Colloid Interface Sci. 486 (2017) 163.
[46] J. Rivera-Utrilla, C.V. Gómez-Pacheco, M. Sánchez-Polo, J.J. López-Peñalver, R. Ocampo-Pérez, J. Environ. Manage. 131 (2013) 16.
[47] C. Gan, Y. Liu, X. Tan, S. Wang, G. Zeng, B. Zheng, T. Li, Z. Jiang, W. Liu, RSC Adv. 5 (2015) 35107.
[48] C. Peiris, S.R. Gunatilake, T.E. Mlsna, D. Mohan, M. Vithanage, Bioresour. Technol. 246 (2017) 150.
[49] X. Zhu, C. Li, J. Li, B. Xie, J. Lü, Y. Li, Bioresour. Technol. 263 (2018) 475.
[50] X. Wang, P. Zhang, C. Wang, H. Jia, X. Shang, J. Tang, H. Sun, J. Hazard. Mater. 424 (2022), 127225.
[51] M.A.O. Lourenço, J. Zeng, P. Jagdale, M. Castellino, A. Sacco, M.A. Farkhondehfal, C.F. Pirri, ACS Sustain. Chem. Eng. 9 (2021) 5445.
[52] W. Wang, M. Gao, M. Cao, J. Dan, H. Yang, Sci. Total Environ. 759 (2021), 143542.
[53] H. Liu, G. Xu, G. Li, J. Colloid Interface Sci. 587 (2021) 271.
[54] S. Chen, C. Qin, T. Wang, F. Chen, X. Li, H. Hou, M. Zhou, J. Mol. Liq. 285 (2019) 62.
[55] M. Chen, C. Bao, D. Hu, X. Jin, Q. Huang, J. Anal. Appl. Pyrol. 139 (2019) 319.
[56] L. Long, Y. Xue, Y. Zeng, K. Yang, C. Lin, J. Clean. Prod. 166 (2017) 1244.
[57] J. Liu, B. Zhou, H. Zhang, J. Ma, B. Mu, W. Zhang, Bioresour. Technol. 294 (2019), 122152.
[58] P. Zhang, Y. Li, Y. Cao, L. Han, Bioresour. Technol. 285 (2019), 121348.
[59] X. Zhu, Y. Liu, F. Qian, C. Zhou, S. Zhang, J. Chen, Bioresour. Technol. 154 (2014) 209.
[60] D. Zhang, Q. He, X. Hu, K. Zhang, C. Chen, Y. Xue, Colloids Surf. Physicochem. Eng. Aspects 615 (2021), 126254.
[61] L.R. de Carvalho Costa, L. de Moraes Ribeiro, G.E.N. Hidalgo, L.A. Feris, Environ Technol 43 (2022) 907.
[62] Y. Cheng, B. Wang, J. Shen, P. Yan, J. Kang, W. Wang, L. Bi, X. Zhu, Y. Li, S. Wang, L. Shen, Z. Chen, J. Hazard. Mater. 432 (2022), 128757.
[63] A. Popova, M. Christov, A. Zwetanova, Corros. Sci. 49 (2007) 2131.
[64] Z. Sun, L. Zhao, C. Liu, Y. Zhen, J. Ma, Environ. Sci. Tech. 53 (2019) 10342.